AGU PUBLICATIONS

JGR

Journal of Geophysical Research: Atmospheres

RESEARCH ARTICLE
10.1002/2015JD023234

**Key Points:**
- Year-round monitoring of marine boundary layer water vapor isotopic composition
- Intraseasonal to interseasonal variability in North Atlantic water vapor isotopes
- Attribution of temporal and spatial variability in water vapor deuterium excess

**Supporting Information:**
- Figures S1–S9 and Tables S1

**Correspondence to:**
H. C. Steen-Larsen,
hanschr@gfy.ku.dk

**Citation:**
Steen-Larsen, H. C., A. E. Sveinbjörnsdottir, Th. Jonsson, F. Ritter, J.-L. Bonne, V. Masson-Delmotte, H. Sodemann, T. Blunier, D. Dahl-Jensen, and B. M. Vinther (2015), Moisture sources and synoptic to seasonal variability of North Atlantic water vapor isotopic composition, *J. Geophys. Res. Atmos.*, *120*, 5757–5774, doi:10.1002/2015JD023234.

Received 9 FEB 2015
Accepted 19 MAY 2015
Accepted article online 21 MAY 2015
Published online 24 JUN 2015



# Moisture sources and synoptic to seasonal variability of North Atlantic water vapor isotopic composition

**H. C. Steen-Larsen[1,2], A. E. Sveinbjörnsdottir[3], Th. Jonsson[3], F. Ritter[1], J.-L. Bonne[1], V. Masson-Delmotte[1], H. Sodemann[4], T. Blunier[2], D. Dahl-Jensen[2], and B. M. Vinther[2]**

[1]Laboratoire des Sciences du Climat et de l'Environnement, UMR CEA-CNRS-UVSQ/IPSL, Gif-sur-Yvette, France, [2]Centre for Ice and Climate, Niels Bohr Institute, University of Copenhagen, Copenhagen, Denmark, [3]Institute of Earth Sciences, University of Iceland, Reykjavik, Iceland, [4]Geophysical Institute, University of Bergen, Bergen, Norway

**Abstract** The isotopic composition of near surface (or planetary boundary layer) water vapor on the south coast of Iceland (63.83°N, 21.47°W) has been monitored in situ between November 2011 and April 2013. The calibrated data set documents seasonal variations in the relationship between $\delta^{18}O$ and local humidity (ppmv) and between deuterium excess and $\delta^{18}O$. These seasonal variations are attributed to seasonal changes in atmospheric transport. A strong linear relationship is observed between deuterium excess and atmospheric relative humidity calculated at regional sea surface temperature. Surprisingly, we find a similar relationship between deuterium excess and relative humidity as observed in the Bermuda Islands. During days with low amount of isotopic depletion (more enriched values), our data significantly deviate from the global meteoric water line. This feature can be explained by a supply of an evaporative flux into the planetary boundary layer above the ocean, which we show using a 1-d box model. Based on the close relationship identified between moisture origin and deuterium excess, we combine deuterium excess measurements performed in Iceland and south Greenland with moisture source diagnostics based on back trajectory calculations to establish the distribution of d-excess moisture uptake values across the North Atlantic. We map high deuterium excess in the Arctic and low deuterium excess for vapor in the subtropics and midlatitudes. This confirms the role of North Atlantic water vapor isotopes as moisture origin tracers.

## 1. Introduction

Measurements of atmospheric water stable isotopes ($H_2{}^{16}O$, $HD^{16}O$, $H_2{}^{18}O$, $H_2{}^{17}O$) provide integrated information related to hydrological cycle processes and offer the potential to constrain associated parameterizations in atmospheric models and potentially improve weather predictions [e.g., *Yoshimura et al.,* 2014; *Gryazin et al.,* 2014].

Due to the different vapor pressure and molecular diffusivities of the water isotopes, ambient environmental parameters, such as temperature and humidity, during occurrence of phase transitions, will leave an imprint on the isotopic composition of the water vapor. Condensation occurs as an air mass undergoes cooling below its dew point, and in terms of the water stable isotopes a distillation process will occur, affecting both the water vapor and precipitation isotopic composition. The water isotopic composition of the vapor in the air mass will therefore represent an integrative tracer for phase-transition and mixing processes.

We use the $\delta$-notation for isotopic ratios introduced by *Craig* [1961]

$$\delta^* = \left(\frac{R_{\text{sample}}}{R_{\text{vsmow}}} - 1\right) \times 1000, \quad (1)$$

where $\delta^*$ represents either $\delta^{18}O$ or $\delta D$, and $R_{\text{sample}}$ and $R_{\text{vsmow}}$ are the isotopic ratio of the sample and Vienna Standard Mean Ocean Water (VSMOW) for the respective isotopic species.

Since the 1960s, the isotopic composition of precipitation has been monitored at a monthly scale by the IAEA [*Rozanski et al.,* 1993]. Moreover, records obtained from Greenland, Antarctic, and glacier ice cores have been used to document past climatic changes [e.g., *Dansgaard et al.,* 1969; *Johnsen et al.,* 1972]. Reconstructions of past local temperature changes from Greenland ice core water stable isotope records still rely on empirical temperature-isotope relationships [e.g., *Vinther et al.,* 2009; *NEEM community members*, 2013] which are time and space dependent [*Guillevic et al.,* 2013; *Kindler et al.,* 2014].

*Craig* [1961] noted that the relationship between $\delta^{18}$O and $\delta$D reflects the influence of kinetic and equilibrium fractionation processes. This led *Dansgaard* [1964] to define a second-order parameter, deuterium excess (hereafter d-excess), which highlights the isotopic variability driven by kinetic fractionation. As global meteoric water is distributed on a line with a slope of 8 in a $\delta$D versus $\delta^{18}$O diagram, the d-excess is defined as the deviation from this line,

$$\text{d-excess} = \delta\text{D} - 8\times\delta^{18}\text{O} \quad (2)$$

Modeling studies suggest d-excess in the boundary layer would be sensitive to evaporation conditions (sea surface temperature (SST), surface relative humidity (RHsst), wind speed regime) and would be modified through nonequilibrium condensation along an air parcel's trajectory. Based on these simple modeling approaches, the Greenland ice core d-excess records have been translated into past changes in moisture source SST and/or RHsst [*Masson-Delmotte et al.,* 2005; *Steen-Larsen et al.,* 2011]. Such theoretical Rayleigh distillation modeling has several caveats such as assuming a single moisture source region, assuming an isotopic closure at the moisture source, and relying on semiempirical parameterizations of kinetic processes that occur during evaporation and snow crystal formation [*Merlivat and Jouzel*, 1979; *Jouzel and Merlivat*, 1984].

The physical processes governing the hydrological cycle in the atmosphere have predominantly been studied using the end product (the precipitation) and were limited by the discontinuity and temporal resolution of precipitation isotopic composition measurements. Recent development of laser spectroscopy has allowed continuous in situ water vapor isotope observations [*Baer et al.,* 2002; *Crosson et al.,* 2002] to provide accurate measurements of the intermediate product (the water vapor). Pioneer multiyear studies based on discrete cryogenic sampling have shown the importance of these water vapor isotopic composition measurements in understanding moisture cycling in the atmosphere [e.g., *Jacob and Sonntag*, 1991; *Angert et al.,* 2008]. Despite the added value of year-round continuous water vapor isotope and d-excess observations, relative few studies have been presented so far [*Welp et al.,* 2012; *Bonne et al.,* 2014; *Bastrikov et al.,* 2014; *Steen-Larsen et al.,* 2014b].

Recent measurements of water vapor isotopes have been carried out in the marine boundary layer from coastal stations or oceanographic cruises, either using cryogenic trapping techniques [*Gat et al.,* 2003; *Uemura et al.,* 2008; *Kurita*, 2011, 2013] or using continuous in situ analyzers [*Steen-Larsen et al.,* 2014b; *Benetti et al.,* 2014]. All these studies have concluded that relative humidity is the dominating factor controlling the water vapor d-excess, in agreement with semitheoretical calculations [*Merlivat and Jouzel*, 1979]. The studies have, however, identified different d-excess/RHsst slopes, which depend on the season and/or transport path. The relative influences of sea surface temperature and wind speed remain however equivocal [*Steen-Larsen et al.,* 2014b]. *Pfahl and Sodemann* [2014] proposed an empirical method to estimate the relation between d-excess and the evaporation conditions based on the few high-resolution vapor observations available at that time. Their results also suggest that the dominant factor determining d-excess in vapor above the ocean surface is the RHsst.

In order to improve understanding of the processes controlling the isotopic composition of Greenland snowfall and improve the interpretation of ice core records, a network of monitoring stations has been implemented along a North Atlantic transect. Based on Greenland ice core d-excess data, combined with Rayleigh modeling, the major moisture source region for central Greenland snowfall was initially suggested to be located in the western subtropical Atlantic Ocean [*Johnsen et al.,* 1989; *Steen-Larsen et al.,* 2011]. This was however challenged by atmospheric modeling, both from water tagging within general circulation models [*Werner et al.,* 2001] and from moisture source identification based on backward trajectories [*Sodemann et al.,* 2008a, 2008b]. These two approaches suggested that the dominant moisture source region for the Greenland ice sheet was located in the North Atlantic, just south of Iceland [*Sodemann et al.,* 2008b]. In order to provide observations of the surface water vapor isotopic composition in potential moisture sources, it was decided to monitor surface water vapor isotopic composition in the subtropical Atlantic (Bermuda islands) [*Steen-Larsen et al.,* 2014b], in the North Atlantic, in South Greenland [*Bonne et al.,* 2014], and Iceland (this study).

The first in situ continuous Arctic measurements were performed during several field seasons at NEEM deep ice core drilling station [*Steen-Larsen et al.,* 2013, 2014a]. Consistent with the work of *Kurita* [2011] in the Siberian Arctic, the NEEM data showed high d-excess values for air masses advected from the Arctic

identified using backward trajectories and water tagging [*Steen-Larsen et al.,* 2013]. These data were also compared with the results of the LMDZiso atmospheric general circulation model equipped with water stable isotopes and nudged to large-scale wind pattern from atmospheric reanalysis products. While LMDZiso correctly captures the observed synoptic variations in temperature, humidity (ppmv), and $\delta^{18}O$, it strongly underestimated the variability of d-excess. This mismatch was understood to reflect either a too low simulated influx of Arctic water vapor or caveats of model parameterization of boundary layer processes leading to a poor representation of physical processes controlling evaporation at the sea ice margin.

A year-round (~13 months) record from coastal South Greenland (Ivittuut 61.21°N, 48.17°W, altitude 30 m above sea level) was also produced [*Bonne et al.,* 2014]. Using Lagrangian moisture source diagnostic, the major moisture source region was identified to be in the North Atlantic. The variability of Ivittuut d-excess was closely related to that of surface relative humidity (RHsst) in an area south of Iceland. This statistical analysis provided empirical support to the idea that the initial d-excess source signal is preserved during transportation toward Ivittuut, at least in the absence of condensational processing involving ice phase, and thereby supporting modeling results [*Jouzel et al.,* 2013]. *Bonne et al.* [2015] combined measurements performed simultaneously in Bermuda, Ivittuut, and NEEM with atmospheric modeling during an exceptional atmospheric river event, which occurred in July 2012 and caused widespread melt across the surface of the Greenland ice sheet [*Neff et al.,* 2014]. They demonstrated that the advection of subtropical moisture identified with a low d-excess signal could be identified up to the NEEM site and confirmed that d-excess conserves a source signal during transportation from the subtropics to NW Greenland.

Here, we expand the record of water vapor isotopic composition in the North Atlantic using new observations performed on the south coast of Iceland (near Selvogsviti) covering more than one year (~16 months). We interpret the new measurements with a focus on the drivers of d-excess variability: What is the relationship between local d-excess and relative humidity at sea surface temperature? Is it similar to that observed in Bermuda and south Greenland? Does it vary by season? Is there an imprint of weather regimes in Iceland water vapor isotopic composition? What is the origin of the moisture and how does it affect d-excess?

The paper is organized into six sections. Section 2 describes the setup, calibration protocol, and methodology. The water vapor isotope record is described and its relationship with local meteorological observations investigated in section 3. The drivers of d-excess are explored in section 4, using meteorological data and moisture transport calculation, including a comparison with the South Greenland data. The main conclusions are reported in section 5, and finally section 6 summarizes the challenges and lessons learned from operating a water vapor isotope analyzer in full autonomous conditions for extended periods of time in harsh conditions.

## 2. Data and Methodology

### 2.1. Instrumental Setup

The water vapor isotope system consists of a Los Gatos Research (LGR) Inc. Water Vapor Isotope Analyzer (WVIA model number 908–0004) together with a LGR Water Vapor Isotope Standard Source (WVISS model number 908-0004-901), which generates water vapor without fractionation from liquid water of known isotopic composition. The system was installed on the Southern Peninsula (Reykjaness), in the SW corner of Iceland, on the top level of a lighthouse (at Selvogsviti, 63.83°N, 21.47°W; Figure 1) located ~50 m from the sea (Figure 1). The lighthouse has an unobstructed path of the Atlantic Ocean and is located within a 5 km flat lava field. Based on the location of the sampling site, we consider wind directions from 90° to 330°N to reflect the ocean sector, while wind directions from 330° and 90°N reflect the land sector (Figure 1).

The installation consists of an upper inlet at the top of the lighthouse (~22 m above the ground) and a lower inlet on the north (lee) side of the lighthouse (~10 m above the ground), where it is shielded from direct sea spray during storms (Figure 1). The two inlets were implemented in order to secure continuous sampling in the case that one of the inlets was damaged. A one fourth inch outer diameter copper tube connecting the inlets with the analyzer was installed inside a 2 cm thick tube insulation material (Armaflex®) protected with a PVC pipe. The PVC pipe was installed to protect the insulation material against degradation. The air intakes

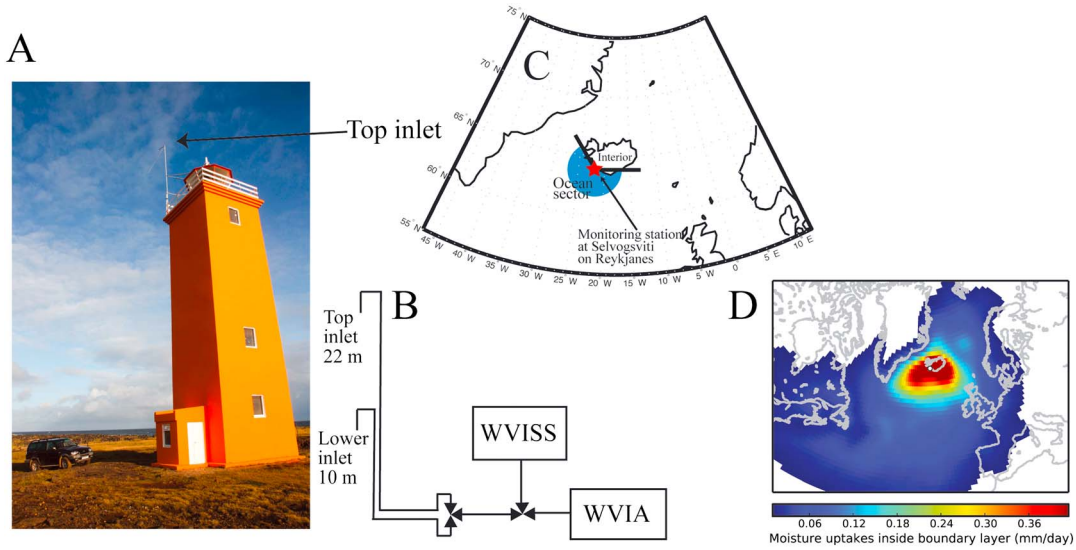


**Figure 1.** (a) Picture of the lighthouse at Selvogsviti in which the system is installed. The top inlet is indicated. (b) Schematic of installation of water vapor isotope measurement system. (c) The map shows the position of the system and the definition of the ocean and interior sector. (d) Daily annual-averaged moisture uptake in the boundary layer for the air parcels arriving at Selvogsviti.

were protected with a cover against sea spray and rain. This was however not sufficient, as we detected a few events when rainfall entered the interior of the sampling tube. These were identified by large differences in humidity (ppmv) measurements between the two inlets, as well as humidity (ppmv) levels significantly above ambient saturation level. The tube was heated to ~50 °C using self-regulating heat trace to prevent condensation. Two three-way solenoid valves and an automatic valve-sequencing program were installed to switch measurements between the top or bottom inlet or from the WVISS calibration system (Figure 1). The routine measurement protocol consisted of sampling vapor from the WVISS for 10 min, followed by five cycles of measurements alternating between the upper and lower inlets every 10 min. The transport of air from the inlets to the analyzer was achieved using a pump (KNF N86 KN.18), operating at a flow rate of 5 L per minute.

### 2.2. Meteorological and Oceanographic Measurements

A weather station Davis Vantage Pro2 was also installed on top of the lighthouse, measuring air temperature (±0.5 °C), relative humidity (±3%), pressure (±1.0 mb), wind speed (±1 m/s), wind direction, rain rate (±0.2 mm), and solar radiation. Our data have been compared with parallel measurements from a weather station operated by the Icelandic road service (Vegagerdin) (~2 km away). Their R. M. Young station reports slightly different precisions (±0.3 °C, ±1% RH, ±0.3 m/s, ±3° direction). Despite a different height and location, no significant difference was observed between the observations at the lighthouse meteorology station and at the road meteorology station for temperature and humidity. The wind speed is however on average ~2 m/s higher at the top of the lighthouse than at the road, consistent with the difference in height and distance to the ocean. We therefore could use data from the road meteorological station to fill in gaps in the lighthouse meteorological record. Finally, daily sea surface temperature data (SST) were obtained from the Aqua MODIS satellite observations over an area subjectively chosen to represent local ocean conditions (~350 × 450 km – 58.5°N to 63°N and 16°W to 24.5 W) directly south of Iceland [*Haines et al.*, 2007; *Acker and Leptoukh*, 2007]. This area is located to the North East of the North Atlantic zone where surface relative humidity was identified to be closely related to the variability of d-excess at Ivittuut, South Greenland (49.4°N to 59.6°N, 41.2°W to 22.5°W).

### 2.3. Calibration

The protocol designed by *Steen-Larsen et al.* [2013] was implemented to treat and reference the water vapor isotope observations to the IAEA VSMOW-SLAP scale (Vienna Standard Mean Ocean Water–Standard Light Antarctic Precipitation). The main corrections are summarized below, as well as the changes that were implemented throughout the multiyear monitoring effort.

The water vapor isotopic composition measured by the laser analyzer is affected by the water vapor concentration, a feature often referred to as a concentration- or humidity-isotope dependency. This humidity-isotope response function is established using the WVISS to generate a constant stream of water vapor with a known isotopic composition, injected at different humidity levels. This humidity-isotope response function varied throughout the measurement campaign, confirming earlier observations [*Steen-Larsen et al.,* 2014b]. As a result, we calibrated the isotope response function every ~3–5 months (supporting information Table S1 and Figure S1), derived a correction function using an eighth-order polynomial fit (with a lower-order polynomial fit for the end parts to avoid end-effects), and interpolated the correction between the results, assuming a linear drift in the humidity-isotope correction for each humidity level. Our results are reported against a reference humidity level of 10,000 ppmv.

We reference our measurements to the international VSMOW-SLAP scale by measuring standards of known isotopic composition. This is carried out during routine maintenance, every 1–2 month, by manually changing the water uptake of the WVISS between the different standards, making sure to reach a stable measurement level before changing to another standard (supporting information Table S1). These standards were themselves calibrated against VSMOW-SLAP at the Isotope laboratory of University of Iceland. We assume a linear drift between the calibrations.

In order to account for the instrumental drift, water vapor generated by the WVISS from a drift-standard bottle is measured for 10 min after each 100 min of ambient air measurements (supporting information Figure S2). The usual drift-standard bottle of the WVISS was replaced by a 5 L glass bottle to allow for continuous remote operation over periods longer than a month. This drift-standard water was sampled at each routine maintenance step, and laboratory liquid isotopic measurements confirmed the stability of its isotopic composition through time. A linear drift is assumed in-between each drift-standard measurement.

Based on the intercomparison of two analyzers during one summer at NEEM, *Steen-Larsen et al.* [2013] estimated the accuracy of measurements produced with this methodology and instrument to be ~0.23‰ for 10 min averages of $\delta^{18}$O, 1.4‰ for 10 min averages of $\delta$D, and 2.3‰ for 10 min averages of d-excess. Here, we report 6-hourly results extracted from 30 min average measurements.

Finally, following earlier studies, we scaled the humidity (ppmv) measured by the LGR instrument to the humidity observation of the weather station (supporting information Figure S3). This is the corrected humidity against which our water isotopic composition is compared in the next sections.

### 2.4. Moisture Source Diagnostic

We characterize the long-range transport of moisture reaching our station using a moisture source diagnostic tool based on Lagrangian backward trajectory calculations [*Sodemann et al.,* 2008b]. The Lagrangian dispersion model Flexpart v8.1 [*Stohl et al.,* 2005] calculates 10 days back trajectories of air parcels starting out from a box over the observing station with a 3 h time step. Back trajectories were calculated for air masses starting out from the Iceland station (Box defined as: 63.64°N, 21.95°W to 64.04°N, 21.05°W and from 0 to 500 meter above ground level) as well as Ivittuut station in south-west Greenland for a comparative study (Box defined as 61.0°N, 48.9° W to 61.4°N, 47.8°W and from 0 to 500 m above ground level). The model is forced by European Center for Medium Range Weather Forecast (ECMWF) ERA-Interim reanalyses [*Rabier et al.,* 2000; *Dee et al.,* 2011] at 1°×1° horizontal resolution, with 60 vertical levels. Sources and sinks of moisture are located where air parcels humidity changes in a 3 h interval. By considering the sequence and the contribution of each moisture source to the total moisture in the air parcels, the moisture source diagnostic provides a quantitative estimate of the moisture source for the total vapor in the air parcels. Further details on the method are given in *Sodemann et al.* [2008b]. Moisture sources are integrated from all air parcel trajectories on a 1°×1° grid for a given time period. Here, we consider only moisture uptake in the boundary layer, which represents the amount of water that is taken up by air parcels within a layer of thickness 1.5 times the diagnosed ECMWF boundary layer height above the surface. The moisture uptake is reported in unites of mm $d^{-1}$ and represents the equivalent height of liquid water column added each day in the air parcels over the grid cell area. Another estimated quantity, termed "moisture transport," represents the total amount of water transported in the air masses to the observation site, again integrated over each grid cell, reported in mm/10 day time period (representing the corresponding height of the liquid water column contained in the air masses).

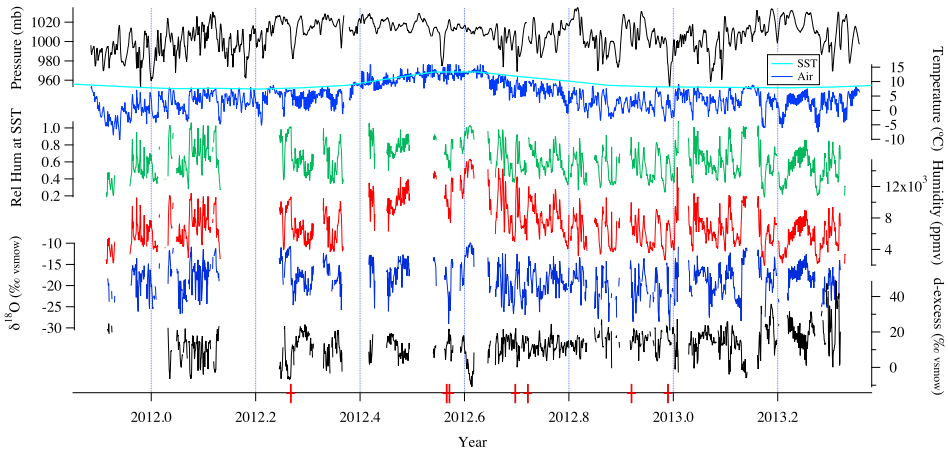


**Figure 2.** Six hour observations during the measurement campaign. (top to bottom) Local atmospheric pressure (mb, black), air temperature (°C, blue) and nearby sea surface temperature (°C, SST, cyan), local relative humidity at sea surface (green), absolute humidity (ppmv, red), $\delta^{18}$O (‰, blue), and d-excess (‰, black). Red crosses in lower panel indicates occurrence of synoptic changes larger than 12‰ in $\delta^{18}$O over 2 days.

## 3. Results

### 3.1. Observations

Figure 2 shows the complete set of 6 h water vapor isotope observations together with local meteorological observations and SST. The observed variability is larger than observed in Bermuda but similar to that observed in South Greenland. It is noted that the data gaps in the record might have a minor effect on the estimated annual mean values (see Table 1).

Despite differences in annual mean temperature, humidity (ppmv), and $\delta^{18}$O/$\delta$D observed at different North Atlantic / Europe / Greenland / Ural stations where year-round vapor isotopic measurements are available, we report comparable annual mean deuterium excess values, within 2.5‰ (Table 2).

In order to characterize the temporal distribution of our Iceland data, histograms of humidity (ppmv), $\delta^{18}$O, $\delta$D, and d-excess are shown in Figure 3. While the $\delta^{18}$O distribution is approximately Gaussian, this is not the case for $\delta$D, a feature further investigated in section 4.2. Seasonal distributions of humidity (ppmv), $\delta^{18}$O, and d-excess (supporting information Figure S4) show similar (and approximately constant) intraseasonal standard deviations for humidity (2000–2400 ppmv) and $\delta^{18}$O (3.2–3.9‰) for all seasons. The $\delta^{18}$O distribution is most skewed for JJA (skewness: −0.52) and least skewed for MAM (skewness: −0.17). The intraseasonal standard deviation of d-excess is minimum in autumn (4.4‰) and maximum in spring (10.6‰).

At the synoptic scale, our record depicts large variations in humidity (ppmv), $\delta^{18}$O, and d-excess within a few days. For example, we observe a ~6000 ppmv increase in humidity over just 24 h on 16 February 2013 (at time 2013.13), associated with a ~15‰ increase in $\delta^{18}$O and ~15‰ decrease in d-excess. This event was

**Table 1.** Annual and Seasonal Mean Values and Standard Deviations for Humidity, $\delta^{18}$O, $\delta$D, and d-excess, Calculated From 6 Hourly Data[a]

| | Annual Mean | Minimum | Maximum | |
|---|---|---|---|---|
| Humidity (ppmv) | 7800 ± 2700 | 2000 (only data above 4000 are used) | 15,000 | |
| $\delta^{18}$O (‰) | −18.4 ± 3.8 | −30.5 | −10 | |
| $\delta$D (‰) | −135 ± 27 | −230 | −85 | |
| d-excess (‰) | 11.4 ± 6.7 | −10 | 50 | |
| | DJF mean | MAM mean | JJA mean | SON mean |
| Humidity (ppmv) | 6500 ± 2000 | 6100 ± 2000 | 10300 ± 2300 | 7400 ± 2400 |
| $\delta^{18}$O (‰) | −18.8 ± 3.9 | −18.0 ± 3.2 | −16.8 ± 3.5 | −19.6 ± 3.3 |
| $\delta$D (‰) | −137 ± 28 | −127 ± 21 | −125 ± 24 | −144 ± 25 |
| d-excess (‰) | 13.3 ± 7.7 | 16.4 ± 10.6 | 9.0 ± 6.2 | 13.2 ± 4.4 |

[a]Note that the distributions are not Gaussian (Figures 3 and S4).

**Table 2.** Mean Values of Temperature, Humidity (ppmv), $\delta^{18}O$, $\delta D$, and d-excess From Stations With d-excess Measurements Covering at Least One Calendar Year[a]

| | Period | Temperature (°C) | Humidity (ppmv) | $\delta^{18}O$ (‰) | $\delta D$ (‰) | d-excess (‰) |
|---|---|---|---|---|---|---|
| Iceland | Jan to Dec 2012 (this study) | ~6.3 | ~7800 | ~ − 18.4 | ~ − 135 | ~11.4 |
| Ivittuut, S. Greenland | Apr 2012 to Mar 2013, no data from Sep and Oct 2012 [*Bonne et al.*, 2014] | ~2.7 | ~7000 | ~ − 22.5 | ~ − 167 | ~12.7 |
| Bermuda, N. Atlantic | Jan to Dec 2012 [*Steen-Larsen et al.*, 2014b] | ~22.9 | ~20500 | ~ − 11.8 | ~ − 81 | ~13.7 |
| Kourovka W. Siberia | Sep 2012 to Aug 2013 [*Bastrikov et al.*, 2014] | ~0.6 | ~8300 | ~ − 25.9 | ~ − 196 | ~11.3 |
| Heidelberg Germany | 1981 to 1987 [*Jacob and Sonntag*, 1991] | 10.1 ± 0.5 | NN | −18.9 ± 0.5 | −140 ± 4 | 11.5 ± 1.1 |

[a]The standard deviation for the measurements at Heidelberg is based on interannual variability.

caused by a passage of a warm front associated with an extratropical cyclone. We identify a subset of eight events during which $\delta^{18}O$ increases or decreases by more than 12‰ within 2 days (red crosses in Figure 2 and supporting information Figure S5). During these events, we observe no systematic relationship between $\delta^{18}O$, local air temperature, and local atmospheric pressure. However, humidity (ppmv) strongly co-varies with $\delta^{18}O$ ($R = 0.62$), while d-excess is anticorrelated with $\delta^{18}O$ ($R = -0.58$). During these synoptic events (Figure 4), the $\delta^{18}O$/humidity slope is $1.5 \times 10^{-3}$‰ ppmv$^{-1}$, almost twice as large as that calculated from observations of synoptic events at Ivittuut ($0.9 \times 10^{-3}$‰ ppmv$^{-1}$). In an idealized situation with a single source this would imply that the station in Iceland is situated further along a distillation path relative to Ivittuut. The d-excess versus $\delta^{18}O$ slope during synoptic events is 2.5 times stronger in Iceland ($-0.76$‰ ‰$^{-1}$) than at Ivittuut (Figure 4). This reflects two different relationships, as indicated by the piecewise linear regression in the right panel of Figure 4, with slopes of approximately $-0.4$‰ ‰$^{-1}$ and approximately $-5$‰ ‰$^{-1}$. No such discontinuity in the relations between d-excess and $\delta^{18}O$ was observed at Ivittuut.

We now focus on the observed seasonal scale. In Iceland, humidity is maximal in summer but minimal in spring. The isotopic species $\delta^{18}O$ and $\delta D$ are most enriched in summer and most depleted in autumn rather than in winter. Deuterium excess is minimum during summer, but at maximum throughout spring, when it is also most variable. This suggests different relationships between $\delta^{18}O$ and humidity throughout different seasons, which may arise from shifts in moisture sources.

Figure 5 displays the $\delta^{18}O$-humidity relationships within individual seasons. The strength of this relationship is smaller in autumn ($R = 0.55$, $n = 284$) and winter ($R = 0.60$ $n = 474$) and larger in spring ($R = 0.75$, $n = 313$) and summer ($R = 0.76$, $n = 278$). We show in Figure S6 in the supporting information the $\delta^{18}O$-humidity relationship together with the RHsst and d-excess variance.

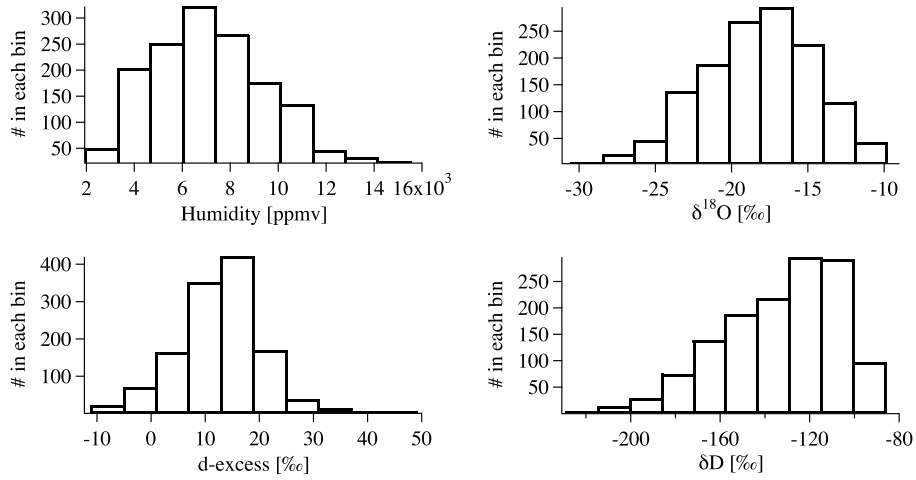


**Figure 3.** Distributions of the 6-hourly observations for humidity (ppmv), $\delta^{18}O$, $\delta D$, and d-excess from the complete campaign.

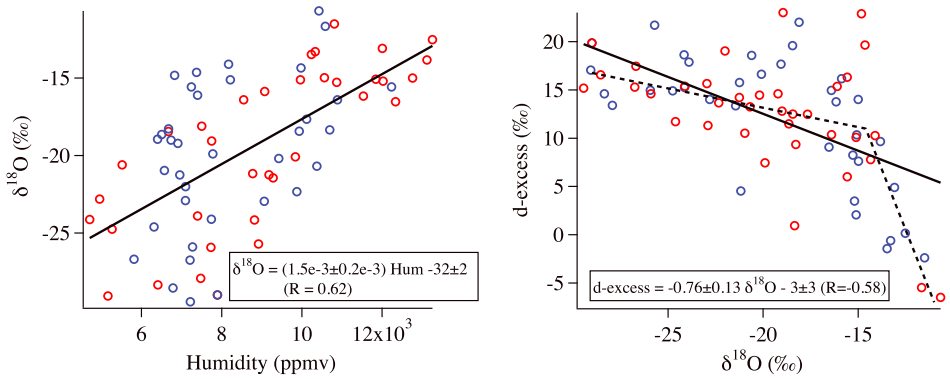


**Figure 4.** The relationship between (left) $\delta^{18}$O and humidity and (right) d-excess versus $\delta^{18}$O for a subset of large synoptic changes. Red circles correspond to synoptic changes that resulted in a decrease in $\delta^{18}$O, while blue circles correspond to those that resulted in an increase in $\delta^{18}$O.

Differences in moisture sources should be apparent in a $\delta$D versus $\delta^{18}$O diagram (Figure 6a, top). The $\delta$D-$\delta^{18}$O slope observed for all Iceland vapor data (6.88 ± 0.05‰ ‰$^{-1}$, $R = 0.96$, $N = 1348$) is similar to that observed at Ivittuut (6.8) [*Bonne et al.,* 2014] and during four spring-summer field seasons at NEEM (6.5–7.4) [*Steen-Larsen et al.,* 2011, 2013, 2014a]. However, the Iceland data reveal a remarkable deviation from the meteoric water line (black solid line, Figure 6a, top) for a subset of points associated with the most enriched $\delta^{18}$O values ($\delta^{18}O > -16$‰). These points lie on a $\delta$D-$\delta^{18}$O slope of ~4.5‰ ‰$^{-1}$ (grey solid line). This subset of data is observed when local relative humidity is close to 100% (color coding) and with southerly winds. Most of our observations are contained within the triangle ABC (Figure 6). The point A is located at $\delta^{18}O = -9.6$‰ and $\delta D = -86.2$‰ (d-excess = −9.4‰), the point B is located at $\delta^{18}O = -16.8$‰ and $\delta D = -106$‰ (d-excess = 28.4‰), and the point C is located at $\delta^{18}O = -28.5$‰ and $\delta D = -212$‰ (d-excess = 16‰).

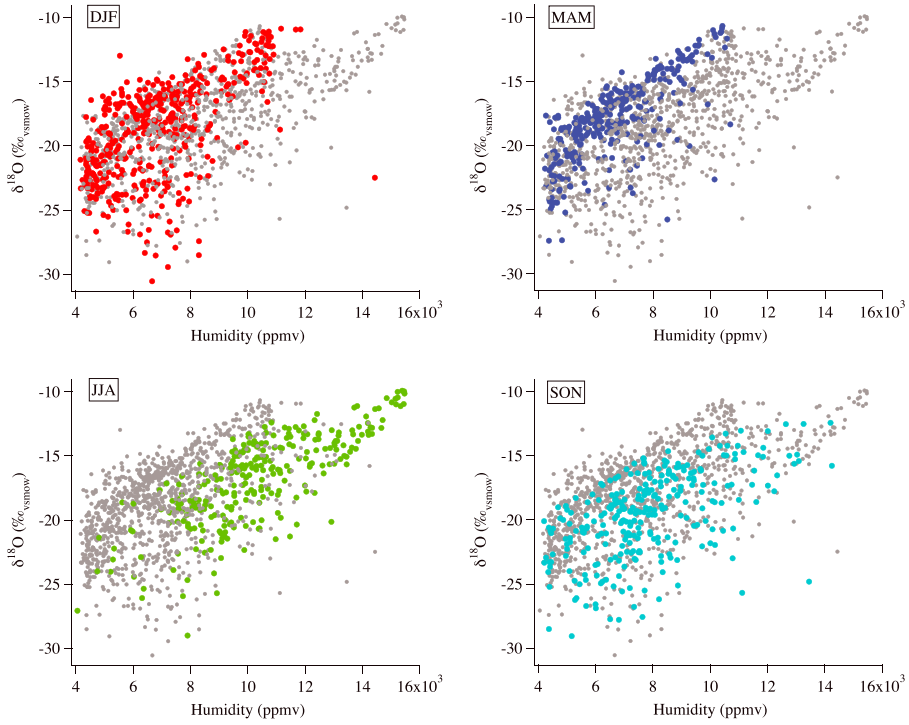


**Figure 5.** Relationship between $\delta^{18}$O and absolute humidity for December-February (DJF, red), March-May (MAM, blue), June-August (JJA, green), and September-November (SON, cyan). The complete set of observations is shown as grey dots in the background.

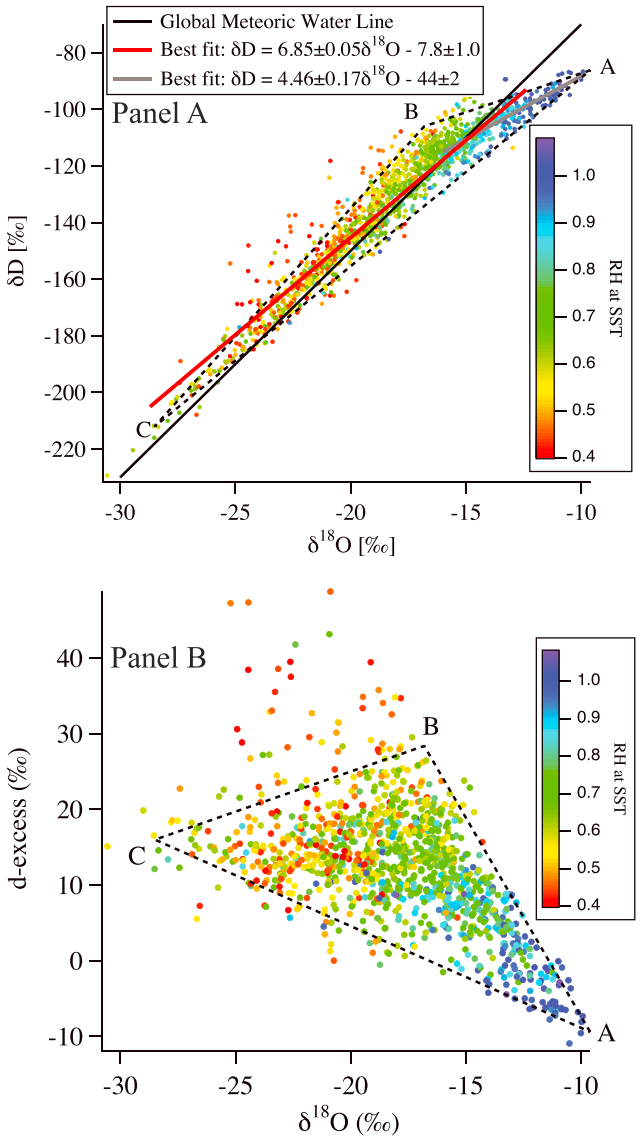


**Figure 6.** The relationship (top) between $\delta$D and $\delta^{18}$O and (bottom) between d-excess and $\delta^{18}$O for all 6-hourly observations. The color code of the dots indicates the concomitant value of the air relative humidity at sea surface temperature. (a) The black solid line indicates the global Meteoric Water Line. The red solid line indicate the best linear fit to the complete data set, and the grey solid line indicate the best linear fit to observations for $\delta^{18}$O greater than −16‰ (Figure 6, top). The letters A, B, and C indicate the corners of the triangle within which most of the observations are distributed.

Due to the shape of the $\delta$D versus $\delta^{18}$O relationship, we expect to identify a similar triangular shape in the observations of the d-excess versus $\delta^{18}$O (Figure 6b, bottom). This is different from earlier reports in Ivittuut [*Bonne et al.,* 2014]. However, the AC line in the d-excess versus $\delta^{18}$O diagram has a slope of $-1.5$‰‰$^{-1}$, which is similar to the average slope observed in Ivittuut ($-1.4$‰‰$^{-1}$) and slightly higher than the average slope observed during the summer campaigns at NEEM ($-1.1$ to $-1.2$‰‰$^{-1}$).

We now investigate the d-excess versus $\delta^{18}$O relationships by season (Figure 7). First, the exceptionally high d-excess values are only observed in spring, when the variance of d-excess is also largest (Figure S4). It is therefore very likely related to long-distance transport also identified in spring (Figure S7). By contrast, the d-excess variance and the d-excess versus $\delta^{18}$O dispersion are both minimum in autumn. During this period, atmospheric transport calculations depict moisture sources mostly located along the most northward part of the North Atlantic. In winter, spring and summer, the data systematically depict a change in d-excess/$\delta^{18}$O relationships for the less depleted $\delta^{18}$O data (above −16‰).

### 3.2. d-excess Versus Relative Humidity

Here, we consider the relative humidity of the atmosphere calculated with respect to the average regional sea surface temperature, $RH_{sst}$. This analysis is therefore restricted to air masses arriving from the ocean sector, excluding air masses advected from the interior of Iceland. The d-excess data are highly scattered for $RH_{sst}$ below 50%, suggesting that, in this case, the local $RH_{sst}$ is not a good predictor of Iceland d-excess. Focusing on the subset of data where $RH_{sst}$ is above 50% (Figure 8), d-excess is closely related to $RH_{sst}$, with a slope of $-0.46 \pm 0.01$‰ %$^{-1}$ (Table 4). It is surprisingly close to the relationship observed at the Bermuda Islands ($-0.43$‰ %$^{-1}$ for all observations) (inset in Figure 8) [*Steen-Larsen et al.,* 2014b].

The similarity of this data with that from the Bermuda Islands (Table 4) is even stronger when considering only observations associated with westerly wind directions (Figure S8). We indeed detect a significant difference in the d-excess versus $RH_{sst}$ slope for westerly winds (180–330°) ($-0.43 \pm 0.02$‰ %$^{-1}$) versus

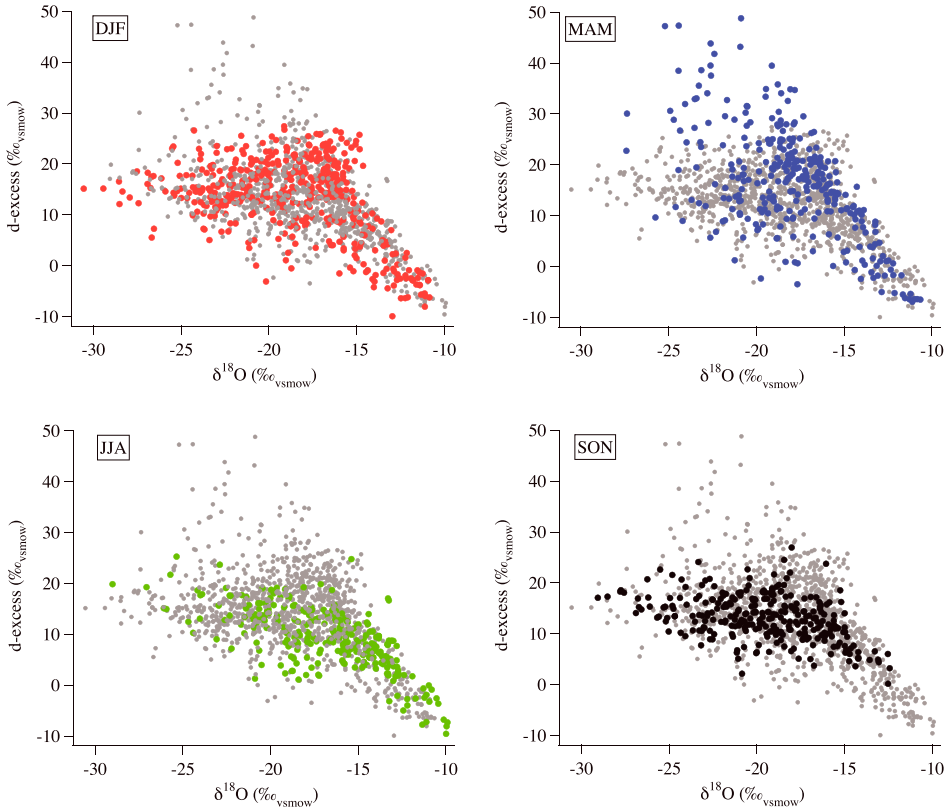


**Figure 7.** Relationship between d-excess and $\delta^{18}$O for December-February (DJF, red), March-May (MAM, blue), June-August (JJA, green), and September-November (SON, black). The complete set of observations is shown in the background as grey dots.

easterly winds (90–180°) ($-0.52 \pm 0.02$‰ %$^{-1}$). We notice that previous cryogenically collected samples reveal a slope of d-excess versus $RH_{SST}$ in the range $-0.58$ to $-0.54$‰ %$^{-1}$ [*Gat et al.*, 2003; *Angert et al.*, 2008; *Uemura et al.*, 2008; *Pfahl and Sodemann*, 2014].

We now compare our results with calculations based on the theoretical approach of *Merlivat and Jouzel* [1979]. First, the slope of the observed relationship is fully consistent with theoretical calculations performed for a smooth ocean regime, independently of the assumed source SST (5 to 20 °C). It is however not compatible with the slope calculated under the hypothesis of a rough ocean evaporation regime. This is confirmed by the lack of any difference in the relationships between d-excess and $RH_{SST}$ when separating the observations into high winds (>7 m/s) and low winds (<6 m/s) (supporting information Figure S9). While our analysis is limited by the fact that our data can reflect both local evaporation and long-distance transport of moisture, we see no support for a significant impact of wind speed on d-excess during evaporation, consistent with our findings from the Bermuda Islands.

Second, we can reproduce the d-excess level and dependence on $RH_{SST}$ from theoretical calculations when assuming a SST of 20 °C, with an ocean surface isotopic composition at VSMOW (0‰ for both $\delta^{18}$O and $\delta$D). Finally, we can only produce the low end observed isotope and d-excess level (point A in Figure 6) for a SST equal to the observed mean temperature of the ocean just south of Iceland (~10 °C) when prescribing the ocean surface isotopic composition to ~1.0‰ for $\delta^{18}$O and ~3‰ for $\delta$D. These values are slightly too enriched compared to recent observations south-west of Iceland: ~0.1–0.3‰ $\delta^{18}$O and ~1–2‰ $\delta$D (M. Benetti, personal communication, 2015).

If Bermuda data were representative of evaporation around Bermuda (at SST of 20–28 °C), and Iceland data were representative of evaporation around Iceland (at SST of around 10 °C), the relationships between d-excess and RH should be parallel for both sites, with at least 5‰ lower d-excess level in Iceland due to the theoretical SST effect. As we observe no such systematic offset (Figure 8), we conclude that either

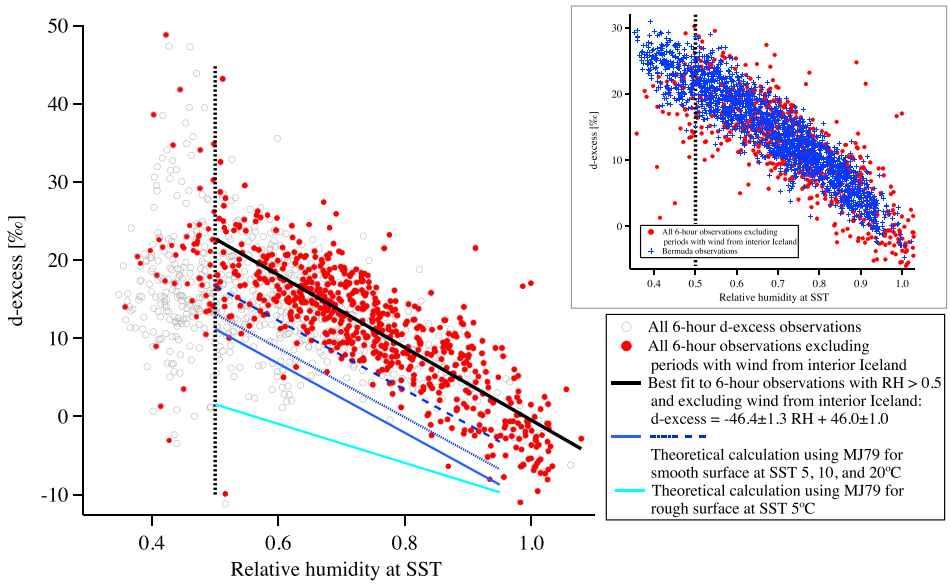


**Figure 8.** Relationship between d-excess and relative humidity at sea surface temperature. All observations are shown as either black circles or red dots. Only air masses that originate from the ocean sector (red dots) and have RHsst $>$ 0.5 are used. Best linear fit to this subset is shown in the black solid line. Theoretical values based on *Merlivat and Jouzel* [1979] (MJ79) is shown for a smooth ocean surface at SST = 5, 10, and 20 °C (blue solid, dotted, and dashed lines). Calculations for a rough ocean surface at 5 °C are shown a cyan solid line. Inset in upper right corner shows observations of the relationship between d-excess and relative humidity at sea surface from Bermuda Islands [*Steen-Larsen et al.,* 2014a, 2014b] as blue crosses together with the observations from Iceland as red dots.

(i) the impact of SST on evaporation d-excess is limited, as also suggested by recent studies [*Pfahl and Sodemann*, 2014; *Steen-Larsen et al.,* 2014b], or (ii) SST controls the amount of atmospheric moisture during air mass cooling and distillation in such a way that $RH_{SST}$ is conserved along air mass trajectories, or (iii) a large fraction of moisture sampled in Iceland arises from long-distance transport from the subtropics, with the exception of the situations where local $RH_{SST}$ is above 0.9, when d-excess strongly decreases. We notice that these scenarios likely are co-occurring and the actual processes will be a combination.

## 4. Discussion

Here, we investigate three aspects. First, we relate the observed relationship between the isotopic composition and the humidity (ppmv) to observations from the Bermuda Islands. Second, we investigate if we can explain theoretically the triangular distribution of $\delta$D versus $\delta^{18}$O, which we believe is observed so far only in Iceland. We propose a simple modeling approach to account for long-distance moisture transport and local evaporation. Third, can we take advantage of the different origins of the Iceland surface vapor to project the d-excess measurements in Iceland onto the different moisture sources? For this last purpose, we combine the in situ measurements with back trajectory calculations and compare the d-excess footprints obtained from Iceland and Greenland measurements.

### 4.1. Isotope-Humidity Relationship

In Figure 5 we reported the $\delta^{18}$O-humidity relationship for individual seasons. Despite large seasonal humidity (ppmv) changes, limited $\delta^{18}$O seasonal variations reflect a changing seasonal $\delta^{18}$O-humidity relationship. We notice that the $\delta^{18}$O versus humidity relationship for DJF and MAM is approximately similar. This is consistent with the moisture transport maps shown in Figure S7 in the supporting information indicating more long-range moisture transport during DJF and MAM compared to JJA and SON. We next explore the reason for the shift in the relationship between $\delta^{18}$O and humidity (ppmv) when comparing DJF with JJA. *Steen-Larsen et al.* [2014b] showed for the Bermuda Islands the mean DJF humidity, $\delta^{18}$O, and d-excess to be ~15,000 ppmv, ~ $-$ 12.7‰, and ~17‰, while the mean JJA humidity,

**Table 3.** Summer and Winter Mean Conditions for the Bermuda Islands

| Bermuda Mean Conditions | DJF | JJA |
|---|---|---|
| Humidity | ~15,000 ppmv | ~26,000 ppmv |
| $\delta^{18}$O | ~ − 12.7‰ | ~ − 10.7‰ |
| d-excess | ~17‰ | ~9‰ |

$\delta^{18}$O, and d-excess was ~26,000 ppmv, ~ − 10.7‰, and ~9‰ (see Table 3). The maximum humidity observed at the station in Iceland in DJF is ~11,000 ppmv, which is only ~4000 ppmv lower than the mean observations at the Bermuda Islands. On the contrary, during JJA the maximum humidity observed in Iceland is approximately ~15,000 ppmv, which is ~11,000 ppmv lower than observations at the Bermuda Islands. Hence, under the conceptual assumption that water vapor observed in Iceland is transported from a region with similar conditions as the region around the Bermuda Islands, a shift in the relationship between $\delta^{18}$O and humidity, consistent with our observations in Figure 5, would be found in Iceland during JJA compared to DJF (relatively more depletion during JJA compared to DJF for similar humidity levels). We notice also a similarity between mean JJA d-excess in Bermuda and Iceland.

### 4.2. Explaining the Triangular Distribution of $\delta$D Versus $\delta^{18}$O

We use here an idealized one dimensional box model based on the Craig-Gordon evaporation model to describe the isotopic flux and humidity uptake when an isolated air mass is only in contact with the ocean surface [*Craig and Gordon*, 1965; *Gat et al.,* 2003]. The model is described in the supporting information.

Using this model, we calculate the evolution of $\delta^{18}$O, $\delta$D, and d-excess of water vapor in response to a continuous uptake of evaporation. We first aim to correctly represent the most enriched values (Point "A" in Figure 6). The isotopic values of water vapor formed in equilibrium with Standard Mean Ocean Water ($\delta^{18}$O = 0‰, $\delta$D = 0‰) at temperatures ranging from 5 to 20 °C are shown as triangles in Figure 9 (Average SST in this region is ~10 °C). The black square (point A) in Figure 9 indicates water vapor in isotopic equilibrium with surface waters at 10 °C and with $\delta^{18}$O of ~1‰ and $\delta$D of ~3‰. However, it is clear from Figure 9 that a precise definition of point "A," and hence, the water vapor in equilibrium with the ocean is difficult due the sparse number of observations at this configuration.

The isotopic evolution of an air mass, starting from point A, is first calculated along a Rayleigh distillation process assuming constant fractionation coefficients (Figure 9, cyan line). This line is approximately parallel with the global meteoric water line (dotted solid line) and represents a bound for the observations on the AC side. Alternatively, we calculate the isotopic evolution of the water vapor when we start out from a

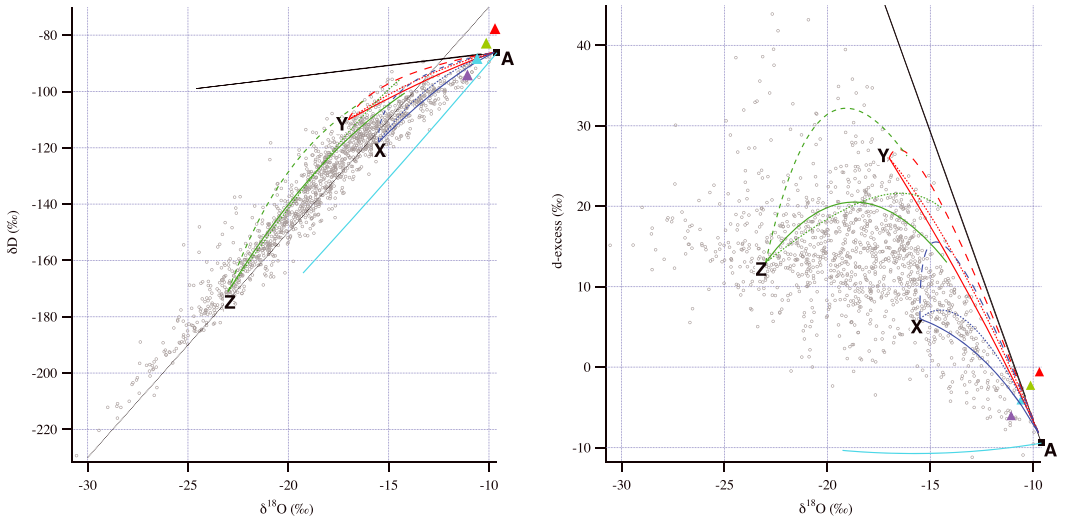


**Figure 9.** Relationship between $\delta$D and $\delta^{18}$O (left) and d-excess versus $\delta^{18}$O (right). Isotopic values in equilibrium with standard mean ocean water are shown with colored triangles, corresponding to calculations for sea surface temperatures at 5 °C (purple), 10 °C (cyan), 15 °C (green), and 20 °C (red). The black square indicates corner A defined in Figures 4 and 5. The global meteoric water line is indicated with a black dotted line in the left panel. The solid cyan line illustrates the calculations of a Rayleigh distillation process for a water vapor mass starting from point A. The black line represents water vapor in a theoretical air mass that is originally completely dry and then filled by only local evaporation.

completely dry air parcel, which is being filled only with the calculated evaporative flux for a SST of ~10 °C (Figure 9, black solid line). This evaporation line provides a bound for the observations on the AB side. It however does not correctly capture the slope of the AB line (the slope of $\delta$D versus $\delta^{18}$O - observed: 2.75 ‰ ‰$^{-1}$, modeled: 0.85 ‰ ‰$^{-1}$ is much shallower than observed, while the slope of d-excess versus $\delta^{18}$O - observed: 5.25 ‰ ‰$^{-1}$, modeled: 6.98 ‰ ‰$^{-1}$ is much steeper). In our simple box model, the slope of the evaporation line strongly depends on the ratio between the kinetic fractionation ($nC_k$ in the model of *Gat* [1996] described in supporting information) of $\delta^{18}$O and $\delta$D but could also be significantly impacted by the introduction of a flux of sea spray assumed to evaporate without fractionation. Reconciling the evaporation line with the observed AB line would require the ratio of the kinetic fractionation for $\delta$D to that for $\delta^{18}$O to increase from 0.87 to 2.6, which appears unrealistic. Using the ocean surface isotopic composition estimated here (based on our point "A"), we tested the inclusion of a flux of sea spray. This in fact enhances the deviation from the observed AB slope. We therefore conclude that the mismatch between the evaporation line and the observed AB slope probably results from the inflow of external water vapor (from the free troposphere), which is not taken into account in our "isolated air mass" box model (assuming that the in-mixing of vapor from the free troposphere would isotopically deplete the vapor of the marine boundary layer).

The water vapor isotopes fall parallel with the meteoric water line and can be explained by a simple Rayleigh distillation. We will now explore a possible cause for the deviation from the meteoric water line toward the corner A (grey solid line in Figure 6a, top). For this purpose, we use the box model to calculate the evolution in the isotopic composition when starting from different initial conditions (isotopic composition and humidity). For illustration purposes, we show the results obtained when starting from point X ($\delta^{18}$O, $\delta$D, d-excess: −15.5‰, −118‰, 6‰, blue lines) and point Y ($\delta^{18}$O, $\delta$D, d-excess: −17.0‰, −116‰, 26‰, red lines), with initial humidity of respectively 60% (dashed lines), 80% (dotted lines), and 90% (solid lines). We find that our observations are consistent with an isotopic evolution starting from point X (at RH = 80% or 90%) and from point Y (at RH = 90%). We therefore conclude that the triangle bracketing our water vapor observations (between the local meteoric water line and corner A is therefore consistent with an isolated air parcel, filled by an ocean evaporative flux given by the formula of Craig-Gordon. Finally, we explore if a similar process could explain high d-excess values. This is illustrated for a calculation starting from point Z ($\delta^{18}$O, $\delta$D, d-excess: −23.0‰, −171‰, 13‰, green lines) with an initial relative humidity of respectively 40% (dashed green line) and 60% (solid green line). Our calculations using the simple box model show a respective d-excess increase of ~20‰ and ~7‰. We conclude that high d-excess observations can be explained by moisture uptake into an isolated air parcel when starting out from low relative humidity and depleted isotopic composition, such as encountered in the high latitudes, when an air mass is moved from being over the continental areas or over the sea ice to being transported over the open ocean.

We conclude that the triangular shape of the distribution of $\delta$D versus $\delta^{18}$O (and d-excess versus $\delta^{18}$O) can be explained in part using a simple box model in which the atmosphere above the ocean is considered isolated and only moistened using an evaporative flux with an isotopic composition given by the formula of Craig-Gordon. We are aware that this is just a simplified idealized description as the model disregards any type of horizontal and vertical mixing with other air masses during transport.

### 4.3. Projecting d-excess Observations at Moisture Sources

Despite the proximity of the monitoring stations on the south coast of Iceland (Selvogsviti, this study) and south Greenland (Ivittuut), about 1300 km, we observe no significant correlation between their isotopic records (both when accounting for and not accounting for transport lag time). This lack of correlation likely results from differences in moisture sources at both synoptic and seasonal time scales. Both sites depict close relationships between observed d-excess and $RH_{SST}$ in the North Atlantic, either locally (close to Iceland) or more remotely (south of Greenland-Iceland for Ivittuut). The annual average moisture uptake pattern for the station in Iceland is shown in Figure 1d, and for the station at Ivittuut shown in supporting information Figure S10. It can be noted that the moisture sources for the station in Iceland are relatively more local (south of Iceland) compared to the moisture sources for Ivittuut (western part of the Atlantic). Ivittuut has a significant moisture contribution from the North American continent, while for Iceland the moisture contribution is predominantly oceanic. There are strong indications that d-excess preserves information related to the initial evaporation conditions [*Jouzel et al.*, 2013; *Pfahl and Sodemann*, 2014]. Unfortunately, this cannot be assessed by direct comparison of observations from Iceland and South

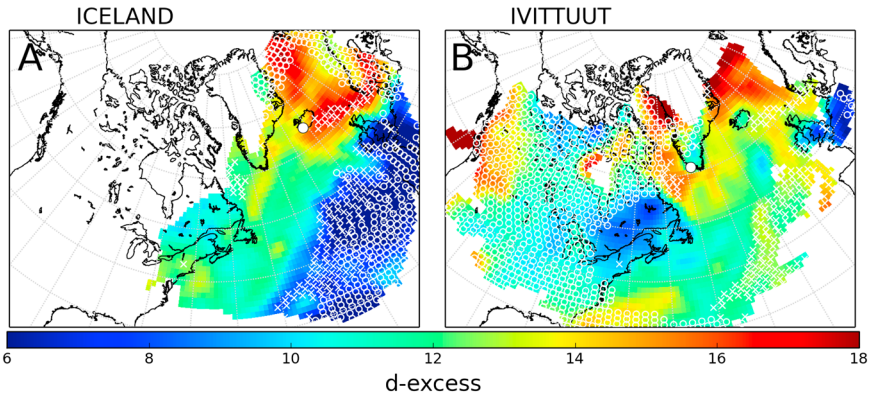


**Figure 10.** The average moisture uptake weighted d-excess pattern based on observations from (a) Selvogsviti, Iceland (this study) and (b) Ivittuut, South Greenland [*Bonne et al.,* 2014]. White circles indicate areas where no overlap of the estimated pattern from the two stations exists. White crosses indicate areas *where the absolute* value of the d-excess pattern from the two stations differs with more than 3‰.

Greenland, as only a few events are associated with back trajectories that pass over both stations. We therefore explore another method to compare the information obtained in Greenland and Iceland, namely, projecting the observed d-excess signal backward to the estimated locations of moisture sources.

We investigate the relationship between the spatial moisture uptake and d-excess observations from the two stations. As described in detail in section 2.4, we calculate the moisture uptake occurring inside the boundary layer on a 1° × 1° grid for both Ivittuut and Selvogsviti stations. We then attribute all observed daily averaged d-excess values to their corresponding location of evaporation. For each 1° × 1° grid cell ($x_m$,$y_n$), we calculate the moisture uptake weighted d-excess value:

$$\text{d-excess}(x_m, y_n) = \frac{\sum_j^{\text{N days}} \text{d-excess}_j \times \frac{\text{moisture uptake}_j(x_m,y_n)}{\sum_{m,n}\text{moisture uptake}_j(x_m,y_n)}}{\sum_j^{\text{N days}} \frac{\text{moisture uptake}_j(x_m,y_n)}{\sum_{m,n}\text{moisture uptake}_j(x_m,y_n)}}, \quad (3)$$

Figure 10 shows maps of this value based on our complete time series. We do not consider possible seasonal variations. For both the Iceland and Greenland data sets, the spatial projections coherently depict a latitudinal gradient, with low d-excess in the Atlantic, and higher d-excess levels around the Arctic (and in the Baffin Bay area). This finding supports earlier results from Siberia [*Kurita*, 2011] and NEEM [*Steen-Larsen et al.,* 2013].

The Iceland projections evidence a longitudinal gradient, with d-excess 6–8‰ higher in the western part of the domain than in the eastern part of the domain. We notice a striking similarity between the longitudinal gradient pattern across the North Atlantic and the predicted spatial evaporated d-excess for DJF based only on reanalysis RH [*Pfahl and Sodemann*, 2014, Figure 2]. Both projections indicate relatively low d-excess levels in moisture originating from the eastern Canada and northeastern USA. We can also validate our approach by comparison of these projections with other in situ measurements, if they are available for the same time period. For instance, the d-excess level estimated for the area around the Bermuda Islands is 12–14‰, which is similar to the annual mean value of 13.7‰ observed for year 2012. We stress that values from the margins of these maps should be interpreted with caution due to limits in the moisture weighted signal.

Finally, this approach can also be used to compare the projected d-excess pattern with the climatology of atmospheric water vapor isotopic composition obtained at the first level of isotope-equipped atmospheric general circulation models. While in principle these models could be used to test the validity of the projection approach, such an investigation is beyond the focus of our study. A climatology of LMDZiso d-excess was discussed in *Bonne et al.* [2014, supplemental Figure B2]. We note that our results depict much larger spatial variations than simulated by the LMDZiso. We also note that the LMDZiso model strongly underestimates the temporal variability of surface water vapor d-excess at Ivittuut and NEEM [*Steen-Larsen et al.,* 2013, 2014a; *Bonne et al.,* 2014]. We speculate that the underestimated low temporal variation in the LMDZiso d-excess is related to the underestimated low spatial variation. We reach this hypothesis because

**Table 4.** Summary of the Best Linear Fits Between d-excess and RHsst Obtained by This and Previous Studies[a]

| | Campaign Length | Data Set | Best Linear Fit |
|---|---|---|---|
| South Iceland (this study) | 500 days (315 days of d-excess observations) | Ocean sector ($N = 630$, $R = 0.81$) | d-excess = $-46.1 \pm 1.3$ RHsst + $45.9 \pm 1.0$ |
| | | Eastern sector ($N = 265$, $R = 0.83$) | d-excess = $-52.4 \pm 2.2$ RHsst + $51.2 \pm 1.7$ |
| | | Western sector ($N = 352$, $R = 0.80$) | d-excess = $-42.5 \pm 1.7$ RHsst + $42.4 \pm 13$ |
| Bermuda [*Steen-Larsen et al.*, 2014b] | 500 days (480 days of d-excess observations) | Complete set | d-excess = $-42.6 \pm 0.4$ RHsst + $43.5 \pm 0.3$ |
| Eastern subtropical North Atlantic [*Benetti et al.,* 2014] | 25 days | Complete set | d-excess = $-45$ RHsst + 42 |
| Southern Ocean [*Uemura et al.,* 2008] | 25 days | Complete set | d-excess = $-58$ RHsst + 51 |
| Global [*Pfahl and Sodemann*, 2014] | Combination | | d-excess = $-54$ RHsst + 48.2 |

[a]Error estimates are provided where available.

we expect that smaller spatial variability in a simulated d-excess pattern will result in simulated smaller temporal d-excess variability. *Bonne et al.* [2014] reported that for the area south of Iceland, the LMDZiso simulated slope of d-excess versus RHsst on daily scale was $-0.5‰\,\%^{-1}$, which is consistent with observations (Table 4). Hence, this could indicate that part of the cause for the simulated d-excess deficiencies is related to the surface humidity fields used to control the water vapor evaporation. Of course it should be kept in mind that the LMDZiso d-excess pattern shown by *Bonne et al.* [2014] is from the lowest model level, while our estimates of moisture uptake are intended to represent the evaporative flux. These variables are not identical and direct comparisons are problematic; however, we do expect some similarity between the d-excess of the evaporative flux and the d-excess from the lowest model level. It is hence not exactly the same variable shown and should be treated with care. However, we do expect that some similarity to exist between the flux d-excess value and the lower grid point d-excess value.

## 5. Conclusion

We have successfully operated an autonomous water vapor isotope analyzer in a lighthouse on the south coast of Iceland between the end of 2011 and the beginning of 2013. Using this data set, we have documented seasonal changes in the relationship between the isotopic composition and ambient humidity (ppmv). We argue that changes in atmospheric water vapor transport pattern and hence changing contributions of ocean evaporation from nearby and remote moisture sources cause these seasonal changes. The relationship between $\delta$D and $\delta^{18}$O is shown to deviate from the meteoric water line on the days when RHsst is highest and $\delta^{18}$O least depleted. As a result, we observe a very unusual triangular distribution pattern for $\delta$D-$\delta^{18}$O and d-excess-$\delta^{18}$O space. This pattern can be explained using a simple box model, where the humidity is increased until reaching saturation with an isotopic flux determined by the equation of *Craig and Gordon* [1965]. We conclude that atmospheric water vapor isotopes document the moisture uptake from the ocean as air parcels are transported toward Iceland.

We find the observed relationship between d-excess and RHsst cannot be captured from the local ocean isotopic composition and SST, and appears surprisingly similar to that observed in the Bermuda Islands [*Steen-Larsen et al.,* 2014a, 2014b]. This implies that a significant fraction of moisture sampled in Iceland might be provided by a subtropical moisture source and/or that the atmospheric processes driving $RH_{SST}$ and d-excess in the extratropical North Atlantic are closely related to those in the subtropical North Atlantic. We suggest that this could indicate that on the mean a significant part of observed water vapor in Iceland has previously been at the area around the Bermuda Islands thereby linking the two sites together. If this conclusion were correct, this would support the hypothesis that a significant moisture source for the Greenland Ice Sheet is found in the midlatitudes of the North Atlantic [*Johnsen et al.,* 1989; *Steen-Larsen et al.,* 2011].

Comparison of mean annual d-excess observations from year-round observations in the North Atlantic, Europe, and Siberia reveals surprising similarity in the magnitude of the d-excess. We notice that the stations compared are connected through the westerlies suggesting a common d-excess signal. Using the assumption that the d-excess signal is conserved through transport and governed by moisture source conditions, we have combined the Iceland and South Greenland (Ivittuut) d-excess observations with back trajectory calculations of moisture uptake to project spatially the moisture uptake weighted d-excess values in the North Atlantic.

This approach highlights large latitudinal and longitudinal gradients, with d-excess increasing from south to north (in contrast with simple interpretations based on SST and calculations performed in accordance with *Merlivat and Jouzel* [1979], which predict d-excess to decrease with decreasing SST) and d-excess decreasing from west to east. These patterns are consistent with the theoretical impact of $RH_{SST}$ on the d-excess at evaporation. The results appear in good agreement with in situ water vapor isotope data from the Bermuda Islands. Despite the fact that the observations from Iceland and South Greenland both are carried out in the temperate North Atlantic region, significant differences exist in the relationship between humidity and $\delta^{18}O$, and d-excess and $\delta^{18}O$. This points to different moisture transport patterns and sources and highlights the complementary information collecting observations at both of these stations.

Variations in ice core isotope d-excess records have previously been interpreted as changes in source region RH and SST. This study together with other recent studies supports the notion that the d-excess signal is conserved during transport and governed by conditions in the source region. However, mounting evidence suggests that the standard parameterization/interpretation needs to be revisited: this study confirms that the dominant control on the marine boundary layer d-excess is the RHsst, but with no detection of an influence from SST or wind speed/surface roughness.

While outside the scope of this study, the observed temporal variation in d-excess and the generated moisture uptake weighted spatial d-excess pattern are expected to be important tools to benchmark and improve the representation of atmospheric hydrological processes in isotope-enabled General Circulation Models.

## 6. Epilogue on Water Vapor Isotope Analyzer Operation in Remote-Harsh Conditions

As probably noted by the reader, our water vapor isotope record is punctuated by several gaps (Figure 2). Our water vapor isotope system was installed in a remote condition without any direct technical support. When problems occurred, they were not always easy to fix, and several trips back and forth between the lighthouse and the laboratory at the University of Iceland could be needed. Initially, we did not have online access, but this was resolved using the 3G cellular network and a directional antenna with signal enhancement. Unfortunately, the cellular network was not always stable in this remote area, and leading to several periods when data download was not possible during a few days. During the installation, we protected our inlet tube and heating cable with closed cell pipe insulation foam. Unfortunately, we discovered that plucking this foam became the favorite hobby for the local sea gulls, leading to disruptions for our electrical wires and inlet tubes. We speculate that the heat trace made the tubing particularly comfortable to sit on. We subsequently (except for a later incident) prevented this by covering all tubes in PVC pipe material. With the position of Iceland on the mid-Atlantic ridge, earthquakes are frequent. On one occasion, an earthquake caused part of our system to fall off the table, thereby pulling out a power cable, which unfortunately resulted in shutdown of the measurement system. In 2010 and 2011, the volcanic eruptions from Eyjafjallajökull and Grimsvötn spread a significant amount of fine-particle ash around Iceland, particularly on the south coast. This caused clogging in our filters, preventing a smooth airflow, leading to fluctuations in cavity pressure, which affected the water vapor isotope measurements. Mirrors had to be frequently cleaned, probably due to the local mixture of sea spray and very fine-grained ash particles. Because the lighthouse room was not sufficiently clean (due to a layer of fine ash), we had to bring the analyzer back to the institute for mirror cleaning. Servicing the instrument during the winter period was complicated by the formation of a ~1 m deep pond on the track leading to the lighthouse. This required us to use a specially build all-terrain 4WD vehicle belonging to the Earth Science Institute of University of Iceland. Finally, wind speeds above 25 m/s are not unusual. In one occasion, this broke our inlet halting our observations for more than a week until it could be repaired.

**Acknowledgments**

To access the data used in this publication, please refer to H. C. Steen-Larsen (hanschr@gfy.ku.dk). The work was supported by the Danish Council for Independent Research–Natural Sciences grant number 09–072689 and 10–092850, the Carlsberg Foundation, the AXA Research Fund, the University of Iceland Research Fund, and RannIs Infrastructure Fund 10/0244 and 120234–0031. We also acknowledge the MODIS mission scientists and associated NASA personnel for the production of the data used in this research effort. We thank the two anonymous referees and the editor very much for the constructive and good comments during the review process.

## References

Acker, J. G., and G. Leptoukh (2007), Online analysis enhances use of NASA Earth science data, *Eos Trans. AGU*, *88*, 14–17, doi:10.1029/2007EO020003.

Angert, A., J. E. Lee, and D. Yakir (2008), Seasonal variations in the isotopic composition of near-surface water vapour in the eastern Mediterranean, *Tellus Ser. B-Chem. Phys. Meteorol.*, *60*, 674–684, doi:10.1111/j.1600-0889.2008.00357.x.

Baer, D. S., J. B. Paul, M. Gupta, and A. O'Keefe (2002), Sensitive absorption measurements in the near-infrared region using off-axis integrated-cavity-output spectroscopy, *Appl. Phys. B*, *75*, 261–265, doi:10.1007/s00340-002-0971-z.

Bastrikov, V., H. C. Steen-Larsen, V. Masson-Delmotte, K. Gribanov, O. Cattani, J. Jouzel, and V. Zakharov (2014), Continuous measurements of atmospheric water vapour isotopes in Western Siberia (Kourovka), *Atmos. Meas. Tech.*, *7*, 1763–1776, doi:10.5194/amtd-7-475-2014.

Benetti, M., G. Reverdin, C. Pierre, L. Merlivat, C. Risi, H. C. Steen-Larsen, and F. Vimeux (2014), Deuterium excess in marine water vapor: Dependency on relative humidity and surface wind speed during evaporation, *J. Geophys. Res. Atmos.*, *119*, 584–593, doi:10.1002/2013JD020535.

Bonne, J. L., V. Masson-Delmotte, O. Cattani, M. Delmotte, C. Risi, H. Sodemann, and H. C. Steen-Larsen (2014), The isotopic composition of water vapour and precipitation in Ivittuut, southern Greenland, *Atmos. Chem. Phys.*, *14*, 4419–4439, doi:10.5194/acp-14-4419-2014.

Bonne, J., et al. (2015), The summer 2012 Greenland heat wave: In situ and remote sensing observations of water vapor isotopic composition during an atmospheric river event, *J. Geophys. Res. Atmos.*, *120*, 2970–2989, doi:10.1002/2014JD022602.

Craig, H. (1961), Isotopic variations in meteoric waters, *Science*, *133*, 1702–1703.

Craig, H., and L. I. Gordon (1965), *Deuterium and oxygen 18 variations in the ocean and the marine atmosphere, in: Stable Isotopes in Oceanographic Studies and Paleotemperatures, July 26–30 1965*, Spoleto, Italy.

Crosson, E. R., et al. (2002), Stable isotope ratios using cavity ring-down spectroscopy: Determination of C-13/C-12 for carbon dioxide in human breath, *Anal. Chem.*, *74*, 2003–2007, doi:10.1021/ac025511d.

Dansgaard, W. (1964), Stable isotopes in precipitation, *Tellus*, *16*, 436–468.

Dansgaard, W., S. J. Johnsen, J. Møller, and C. C. Langway Jr. (1969), One thousand centuries of climatic record from Camp Century on the Greenland ice sheet, *Science*, *166*, 377–381.

Dee, D. P., et al. (2011), The ERA-Interim reanalysis: Configuration and performance of the data assimilation system, *Q. J. R. Meteorol. Soc.*, *137*, 553–597, doi:10.1002/qj.828.

Gat, J. R. (1996), Oxygen and hydrogen isotopes in the hydrologic cycle, *Annu. Rev. Earth Planet. Sci.*, *24*, doi:10.1146/annurev.earth.1124.1141.1225.

Gat, J. R., B. Klein, Y. Kushnir, W. Roether, H. Wernli, R. Yam, and A. Shemesh (2003), Isotope composition of air moisture over the Mediterranean Sea: An index of the air-sea interaction pattern, *Tellus Ser. B-Chem. Phys. Meteorol.*, *55*, 953–965.

Gryazin, V., C. Risi, J. Jouzel, N. Kurita, J. Worden, C. Frankenberg, V. Bastrikov, K. Gribanov, and O. Stukova (2014), To what extent could water isotopic measurements help us understand model biases in the water cycle over Western Siberia, *Atmos. Chem. Phys.*, *14*, 9807–9830, doi:10.5194/acp-14-9807-2014.

Guillevic, M., et al. (2013), Spatial gradients of temperature, accumulation and $\delta^{18}$O-ice in Greenland over a series of Dansgaard–Oeschger events, *Clim. Past*, *9*, 1029–1051, doi:10.5194/cp-9-1029-2013.

Haines, S. L., G. J. Jedlovec, and S. M. Lazarus (2007), A MODIS sea surface temperature composite for regional applications, *Geosci. Remote Sens., IEEE Trans. on*, *45*, 2919–2927, doi:10.1109/tgrs.2007.898274.

Jacob, H., and C. Sonntag (1991), An 8-year record of the seasonal variation of $^{2}$H and $^{18}$O in atmospheric water vapour and precipitation at Heidelberg, Germany, *Tellus*, *43B*, 291–300.

Johnsen, S. J., W. Dansgaard, H. B. Clausen, and C. C. Langway Jr. (1972), Oxygen isotope profiles through the Antarctic and Greenland ice sheets, *Nature*, *235*, 429–434.

Johnsen, S. J., W. Dansgaard, and J. W. C. White (1989), The origin of Arctic precipitation under present and glacial conditions, *Tellus B*, *41*, 452–468.

Jouzel, J., and L. Merlivat (1984), Deuterium and oxygen 18 in precipitation: Modeling of the isotopic effects during snow formation, *J. Geophys. Res.*, *89*, 11,749–11,757, doi:10.1029/JD089iD07p11749.

Jouzel, J., G. Delaygue, A. Landais, V. Masson-Delmotte, C. Risi, and F. Vimeux (2013), Water isotopes as tools to document oceanic sources of precipitation, *Water Resour. Res.*, *49*, 7469–7486, doi:10.1002/2013WR013508.

Kindler, P., M. Guillevic, M. Baumgartner, J. Schwander, A. Landais, and M. Leuenberger (2014), Temperature reconstruction from 10 to 120 kyr b2k from the NGRIP ice core, *Clim. Past*, *10*, 887–902, doi:10.5194/cp-10-887-2014.

Kurita, N. (2011), Origin of Arctic water vapor during the ice-growth season, *Geophys. Res. Lett.*, *38*, L02709, doi:10.1029/2010GL046064.

Kurita, N. (2013), Water isotopic variability in response to mesoscale convective system over the tropical ocean, *J. Geophys. Res. Atmos.*, *118*, 10,376–10,390, doi:10.1002/jgrd.50754.

Masson-Delmotte, V., et al. (2005), Holocene climatic changes in Greenland: Different deuterium excess signals at Greenland Ice Core Project (GRIP) and NorthGRIP, *J. Geophys. Res.*, *110*, D14102, doi:10.1029/12004JD005575.

Merlivat, L., and J. Jouzel (1979), Global climatic interpretation of the deuterium-oxygen 18 relationship for precipitation, *J. Geophys. Res.*, *84*, 5029–5033, doi:10.1029/JC084iC08p05029.

NEEM community members (2013), Eemian interglacial reconstructed from a Greenland folded ice core, *Nature*, *493*, 489–494, doi:10.1038/nature11789.

Neff, W., G. P. Compo, F. Martin Ralph, and M. D. Shupe (2014), Continental heat anomalies and the extreme melting of the Greenland ice surface in 2012 and 1889, *J. Geophys. Res. Atmos.*, *119*, 6520–6536, doi:10.1002/2014JD021470.

Pfahl, S., and H. Sodemann (2014), What controls deuterium excess in global precipitation?, *Clim. Past*, *10*, 771–781, doi:10.5194/cp-10-771-2014.

Rabier, F., H. Järvinen, E. Klinker, J. F. Mahfouf, and A. Simmons (2000), The ECMWF operational implementation of four-dimensional variational assimilation. I: Experimental results with simplified physics, *Q. J. R. Meteorol. Soc.*, *126*, 1143–1170, doi:10.1002/qj.49712656415.

Rozanski, K., L. Araguás-Araguás, and R. Gonfiantini (1993), Isotopic patterns in modern global precipitation, in *Climate Change in Continental Isotopic Records, Geophys. Monogr. Ser.*, vol. 78, pp. 1–36, AGU, Washington D. C.

Sodemann, H., V. Masson-Delmotte, C. Schwierz, B. M. Vinther, and H. Wernli (2008a), Interannual variability of Greenland winter precipitation sources: 2. Effects of North Atlantic Oscillation variability on stable isotopes in precipitation, *J. Geophys. Res.*, *113*, D12111, doi:10.1029/2007JD009416.

Sodemann, H., C. Schwierz, and H. Wernli (2008b), Interannual variability of Greenland winter precipitation sources: Lagrangian moisture diagnostic and North Atlantic Oscillation influence, *J. Geophys. Res.*, *113*, D03107, doi:10.1029/2007JD008503.

Steen-Larsen, H. C., et al. (2011), Understanding the climatic signal in the water stable isotope records from the NEEM shallow firn/ice cores in northwest Greenland, *J. Geophys. Res.*, *116*, D06108, doi:10.1029/2010JD014311.

Steen-Larsen, H. C., et al. (2013), Continuous monitoring of summer surface water vapor isotopic composition above the Greenland Ice Sheet, *Atmos. Chem. Phys.*, *13*, 4815–4828, doi:10.5194/acp-13-4815-2013.

Steen-Larsen, H. C., et al. (2014a), What controls the isotopic composition of Greenland surface snow?, *Clim. Past*, *10*, 377–392, doi:10.5194/cp-10-377-2014.

Steen-Larsen, H. C., A. E. Sveinbjörnsdottir, A. J. Peters, V. Masson-Delmotte, M. P. Guishard, G. Hsiao, J. Jouzel, D. Noone, J. K. Warren, and J. W. C. White (2014b), Climatic controls on water vapor deuterium excess in the marine boundary layer of the North Atlantic based on 500 days of in situ, continuous measurements, *Atmos. Chem. Phys.*, *14*, 7741–7756, doi:10.5194/acp-14-7741-2014.

Stohl, A., C. Forster, A. Frank, P. Seibert, and G. Wotawa (2005), Technical note: The Lagrangian particle dispersion model FLEXPART version 6.2, *Atmos. Chem. Phys.*, *5*, 2461–2474, doi:10.5194/acp-5-2461-2005.

Uemura, R., Y. Matsui, K. Yoshimura, H. Motoyama, and N. Yoshida (2008), Evidence of deuterium excess in water vapor as an indicator of ocean surface conditions, *J. Geophys. Res.*, *113*, D19114, doi:10.1029/2008JD010209.

Vinther, B. M., et al. (2009), Holocene thinning of the Greenland ice sheet, *Nature*, *461*, 385–388, doi:10.1038/nature08355.

Welp, L. R., X. Lee, T. J. Griffis, X.-F. Wen, W. Xiao, S. Li, X. Sun, Z. Hu, M. Val Martin, and J. Huang (2012), A meta-analysis of water vapor deuterium-excess in the midlatitude atmospheric surface layer, *Global Biogeochem. Cycles*, *26*, GB3021, doi:10.1029/2011GB004246.

Werner, M., M. Heimann, and G. Hoffmann (2001), Isotopic composition and origin of polar precipitation in present and glacial climate simulations, *Tellus B*, *53*, 53–71.

Yoshimura, K., T. Miyoshi, and M. Kanamitsu (2014), Observation system simulation experiments using water vapor isotope information, *J. Geophys. Res. Atmos.*, *119*, 7842–7862, doi:10.1002/2014JD021662.